Experimental study on energy dissipation in a 1 kW arcjet thruster

Heji Huang*, Wenxia Pan, Chengkang Wu

Institute of Mechanics, Chinese Academy of Sciences, Beijing 100190, China

*E-mail of presenting author: huang@imech.ac.cn

Abstract As a simple and reliable propulsion system, arcjet thrusters have been used in multiple satellite missions. In order to improve the efficiency of arcjet thrusters, energy dissipation study was carried out in a 1 kW arcjet thruster with pure N_2, H_2-N_2 and H_2 as the propellant. Using a 698 nm interference filter, thermal radiation was isolated from arc and plume emissions and the internal nozzle temperature was obtained by converting the thermal radiation signals. Results show that the addition of hydrogen leads to higher nozzle temperature, which is the determining factor for the mode of arc root attachment. At lower nozzle temperatures, constricted type attachment with unstable motions of the arc root was observed, while a fully diffused and stable arc root was observed at elevated nozzle temperatures. Output energy distribution analysis shows that losses from frozen flow and exhaust thermal losses are the main parts in limiting the efficiency of arcjet thrusters.

Keywords arcjet thruster, performance, energy dissipation

1. Introduction

Power consumption and propulsive efficiency are important parameters in evaluating the performance of a propulsion system. From this aspect, compared to conventional chemical propulsion methods, such as chemical rockets, electric propulsion system is more advanced with higher specific impulse (I_{sp}), higher thrust efficiency, better controllability and longer operating duration, etc..[1, 2] According to the Tsiolkovsky rocket equation, higher I_{sp} is favorable for increasing the ratio of payload mass to total launch mass. However, from the view of energy consumption, an optimized I_{sp} is needed to balance the total power requirement and the propellant consumption for certain space missions where a specific velocity change of the vehicle (ΔV) is needed. Propulsion system with very high I_{sp}, eg. an ion thruster, is usually expected for high ΔV missions, such as deep space explorations. On the other hand, for some satellite missions including north-south station-keeping and orbital maneuvering, arcjet thruster with moderate I_{sp} and relatively larger thrust level is preferred.

An arcjet thruster uses arc discharge to heat the injected propellant, With a de Laval nozzle, the heated propellant is further accelerated and exhausted to generate the required thrust. The performance of an arcjet thruster is controlled by the characteristics of the arc discharge behavior and the arc-electrode interactions to a large extent. Generally, the anode of an arcjet thruster also acts as the de Laval nozzle, which makes it a key component. It is in the anode/nozzle that the conversion of thermal energy into directed kinetic energy occurs. In order to improve the performance of an arcjet thruster, it is essential to understand the physical processes inside the anode/nozzle better.

In this research, energy dissipation mechanisms in the anode/nozzle of a 1kW arcjet thruster with propellant of N_2, H_2-N_2, and H_2 were analyzed based on time-dependent monitoring of arcjet operating parameters and performances, including arc current, voltage, nozzle temperature, propellant flow rate, arc-root attachment and the obtained thrust.

2. Experimental conditions

All the experiments were carried out in ESAPD (Experimental System of Aerospace Plasma Dynamics) in the Institute of Mechanics, Chinese Academy of Sciences. The vacuum chamber of ESAPD is 2 meters in diameter and 4 meters in length with an ultimate vacuum of 10^{-4} Pa. Details of the ESAPD system can be found in ref. [3] Based on previous experimental scheme in studying arc root behavior in a specially designed non-transferred dc plasma torch operated at reduced pressure [4], continuous monitoring of the images inside the thruster nozzle was done by a high-speed-video camera (HSVC) or a conventional video camera (Sony, DSR-PD198P). The nozzle of the arcjet thruster was regeneratively cooled with a throat diameter of 0.7 mm and an exit diameter of 11 mm. The outside nozzle temperature was measured by two infrared pyrometers with a combined measuring range of 473 – 2273 K. A 45° tilted copper mirror was used to reflect the end-on view of the nozzle to the outer HSVC. The HSVC was coupled to a telephoto lens with focal length of 200 mm. A 698 nm, 10 nm bandwidth interference filter was mounted on the telephoto lens such that thermal radiation can be isolated from arc and plume emissions. Intensity calibration was performed by monitoring the intensity and temperature of the outside nozzle surface simultaneously. The obtained thermal radiation intensity from the internal surface of the nozzle was then converted to temperature signals. Under current experimental conditions, an internal nozzle temperature from 1200 - 3000 K can be distinguished.

In the present study, the camera speed and exposure time were chosen such that the intensity of the images will not saturate. The obtained kinetic series of images were then analyzed by the software of ImageJ (National Institute of Health. USA). Pure nitrogen, pure hydrogen or nitrogen-hydrogen mixture with volume ration of 1:2 was fed into the arcjet as the propellant. Typical experimental conditions are listed in Table 1.

Table 1 Typical experimental conditions

Propellant	N_2	H_2	H_2:N_2 =2:1
Mass flow rate (mg/s)	83	12	36
Arc current (A)	8	8	8
Arc voltage (V)	99	109	101

End-on view of the nozzle shows concentric circles which represent the edges of the nozzle and the throat, as being illustrated in Fig. 1 (a). The surface of the expanding cavity is between circle 1 and 2. The converging section is not visible in the end-on view image (A-A view in Fig. 1 (a)). With an auxiliary halide lamp, such end-on view image of the nozzle before arcjet ignition was taken. In this case, the interference filter was not applied. The outer circle is the edge of the nozzle exit and the central dark spot represents the throat.

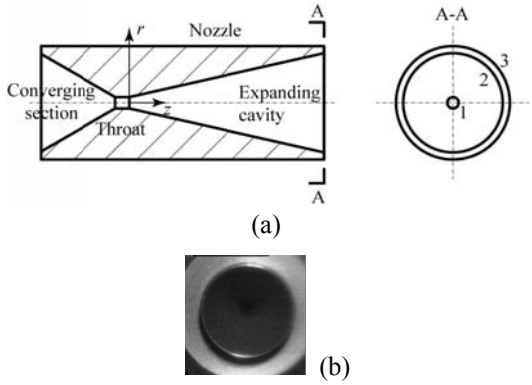

(a)

(b)

Fig. 1 End-on view of the nozzle. (a) illustration and (b) photo taken before ignition with an auxiliary halide lamp.

3. Results and discussions

Time-dependent nozzle temperature change largely depends on the type of the propellant injected. At similar input power levels, as listed in Table 1, the change of outside nozzle temperature with time are shown in Fig. 2. The temperature below 473 K is fitted from the measured data.

With pure nitrogen of 83 mg/s as the propellant, the outside nozzle temperature increases much slower than that when hydrogen is added. It takes more than 5 minutes for the outside nozzle temperature to reach a relative equilibrium outside nozzle temperature of 1220 K. With the mixture of H_2-N_2 as the propellant, the outside nozzle temperature increases much faster, and reaches 1700 K after 5 minutes of ignition, which is about 500 K higher than that when pure N_2 was used. With pure H_2 as the propellant, the outside nozzle temperature increases even faster. It takes only 2 minutes for the outside nozzle temperature to reach a relative equilibrium value of 1600 K. These results suggest that with higher thermal conductivity of hydrogen, the heat transfer from the plasma to the nozzle increases.

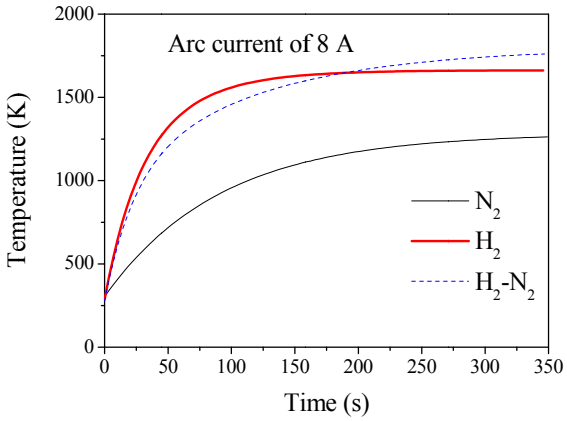

Fig. 2 Change of outside nozzle temperature with time.

Using the 698 nm interference filter, the internal nozzle temperature was obtained. Unlike the arc root movements, the internal nozzle surface temperature is a relative slow response parameter, therefore a conventional video camera which is able to record video clips at 25 fps with much longer time than the HSVC was used to obtain time-dependent internal nozzle thermal radiation signals. Radial profiles of internal temperature distributions are shown in Fig. 3. The radial position represents the r direction illustrated in Fig. 1 (a).

In the present study, the optical path was set such that the cathode tip in the converging section of the nozzle is not visible in the video clip, therefore the center region in Fig. 3 where $r < 0.35$ mm represents the surface temperature of the throat. At the ignition stage, although arc root sometimes moves out of the throat, the temperature at the throat surface cannot follow the random movement of the arc root. Temperature profiles only represent time-averaged values. Therefore, there are no high temperature zones at the ignition stage when the arc root stays mainly upstream of the throat. When pure N_2 was used as the propellant, the high

temperature zone can be seen in the video about 20 seconds after the ignition. The plot representing the temperature distribution of 20 s after the ignition in Fig. 3 (a) shows that the high temperature zone is still inside the throat and there is an asymmetry of the temperature distribution because of the constricted type of the arc root attachment.

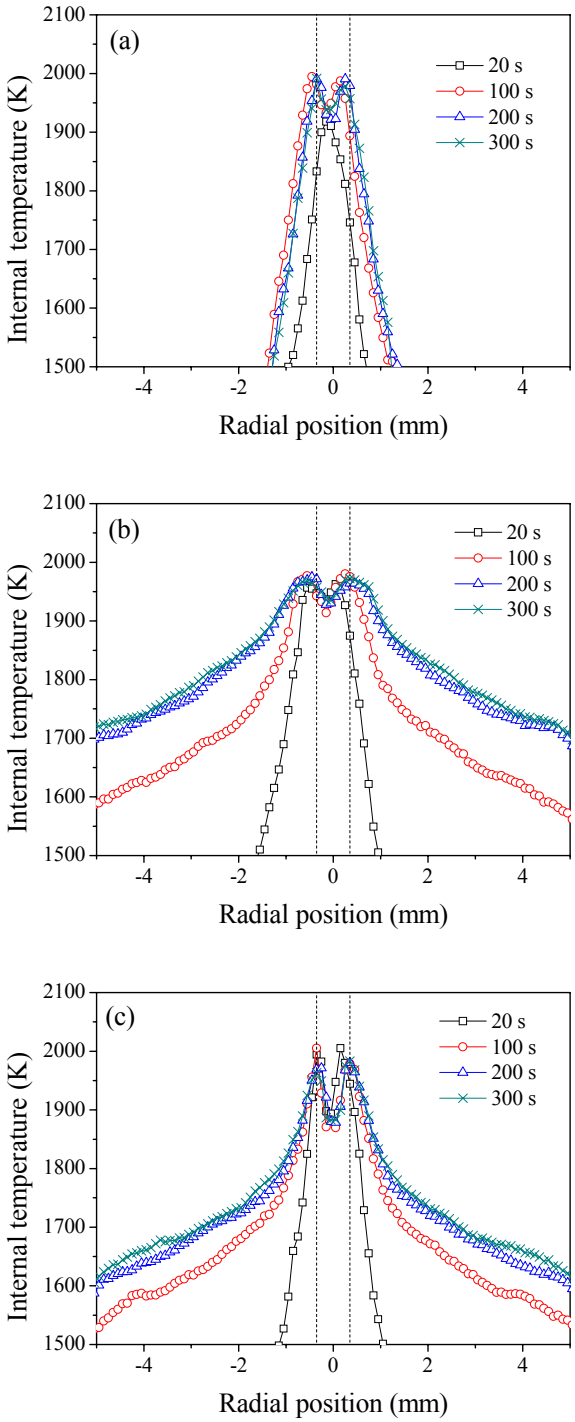

Fig. 3 Time-dependent internal nozzle temperature distributions using (a) pure N_2 (b) H_2-N_2 and (c) pure H_2 as propellant.

As the nozzle temperature increases with time, the high temperature zone moves outwards to the exit of the throat and the surface temperature inside the throat becomes relatively lower comparing with the highest temperature region. Therefore, there are two crests in the radial profile of the internal temperature. When hydrogen is added in, the nozzle temperature increases much faster, and the high temperature zone is seen in the video much earlier than the one when pure N_2 was used. It is about 12 s and 10 s for the case of using H_2-N_2 and H_2 as the propellant, respectively.

Because the plume emission has been cut off by the 698 nm interference filter, the high temperature zone shown in Fig. 3 are mainly caused by the arc root attachment, where Joule heat remarkably increases the surface temperature. And the width of the high temperature zone can reveal the degree of constriction of the arc root attachment qualitatively. No matter what kind of propellants were used, the high temperature zone stays near the exit of the throat at stably working condition, indicating that the arc root attachment position is also on the surface of the nozzle expanding section near the throat exit. Through Fig. 3 (a) - (c), similar trend of the arc root attachment position moving from the upstream of the throat in the ignition stage to the downstream of the throat at stably working condition is confirmed, especially when H_2-N_2 was used as the propellant, a clear expanding of the high temperature zone with time can be seen. With such an expanding of the arc root attachment area, the highest temperature also decreases with time, meaning that the diffused type arc root attachment can reduce local temperature of the nozzle and might be beneficial for alleviating anode erosion.

Fig. 3 also shows that the propellant compositions affect the arc root attachment remarkably. When the outside nozzle temperature are similar in Fig. 3 (b) and (c), the arc root attachment area is much narrower when pure H_2 was used.

With different propellants, the performance of the arcjet thruster varies a lot. The thrust, specific impulse and efficiency at stably working condition are listed in Table 2.

Table 2 Thruster performance

Propellant	N_2	H_2	H_2:N_2 =2:1
Specific power (J/mg)	9.5	73	22
Thrust (mN)	210	74	166
Specific impulse (s)	258	629	471
Efficiency (%)	23.5	18.8	42

The highest specific impulse of 629 s was achieved when pure H_2 is used as the propellant because hydrogen is so light in mass. The highest thrust efficiency of 42% was observed when using H_2-N_2 as the propellant.

According to the measured nozzle temperature distribution on both outside and inside surfaces of the nozzle and the geometry of the thruster, the radiation loss was calculated. Compared to the large area of outside surfaces, the radiation from the inside surface of nozzle is negligible. Taking in the 300 s profiles shown in Fig. 3, the radiation losses from the internal surface of the nozzle are shown in Fig. 4. Although the high temperature zone is close to the exit of the throat, the radiation loss near this area is small because the diameter of the radiation surface here is also small. The total radiation losses from the internal surface of the nozzle are 2.7, 5.9 and 7.5 W for N_2, H_2 and H_2-N_2 propellant respectively. At the same time, the radiation losses from the outside surfaces are 58, 99 and 129 W. So, the part of radiation loss from the internal surface is less than 6 % of the total radiation loss.

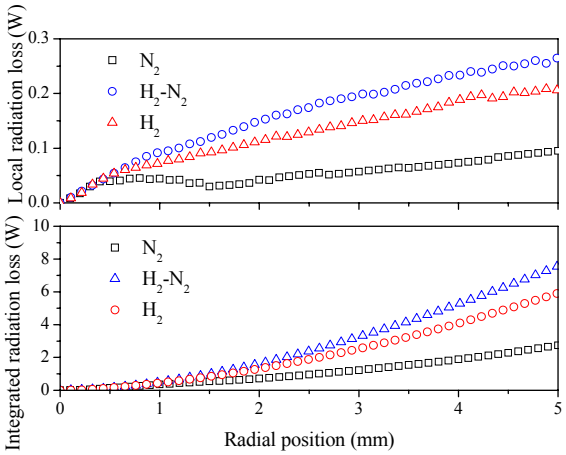

Fig. 4 Local radiation loss (up) and integrated radiation loss (down) from the internal surface of the nozzle.

Output energy distributions for thrust, radiation loss and other losses are plotted in Fig. 5. It is shown that with higher nozzle temperature, the radiation loss increases rapidly. However the total radiation loss is usually less than 20 % of the input energy. When pure N_2 or H_2 were used as the propellant, other losses from frozen flow and exhaust thermal losses are larger than 60 %. An optimization of input power, propellant type and propellant mass flow rate is needed to achieve better performance of arcjet thrusters.

4. Conclusions

Relationships among propellant composition, nozzle temperature and arc root behavior were established. Hydrogen addition greatly affects the nozzle temperature and the arc root attachment area. Nozzle temperature plays an important role in affecting the arc root attachment mode. Higher nozzle temperature promotes diffused type attachment while constricted type attachment occurs at lower nozzle temperatures. Radiation loss from the internal surface of the nozzle is less than 6 % of the part from outside surface and the total radiation loss is usually less than 20 % of the input energy. Frozen flow and exhaust thermal losses are the main parts of energy losses in the studied arcjet thruster. In order to improve the performance of arcjet thruster, an optimization of input power, propellant type and propellant mass flow rate is needed.

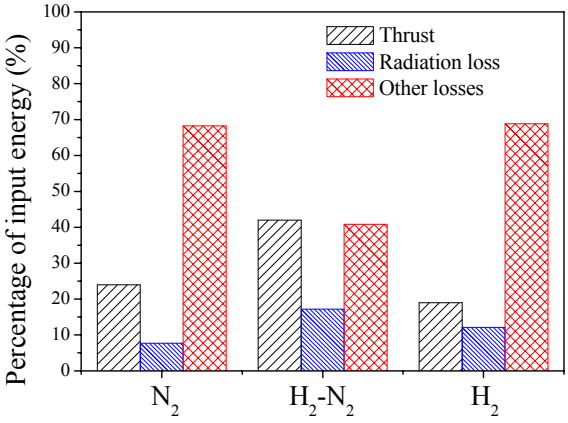

Fig. 5 Output energy distributions for (a) pure N_2 (b) H_2-N_2 and (c) pure H_2 arcjet thrusters.

Acknowledgements

This work is supported by the National Natural Science Foundation of China under Grant Nos. 50836007 and 10921062.

References

[1] G. Saccoccia and W. Berry, "European electric propulsion activities and programmes," *Acta Astronautica,* vol. 47, pp. 193-203, Jul-Nov 2000.

[2] G. W. Butler and R. J. Cassady, "Directions for arcjet technology development," *Journal of Propulsion and Power,* vol. 12, pp. 1026-1034, Nov-Dec 1996.

[3] W. Pan, *et al.*, "Effect of Nozzle Temperature on the Performance of a 1 kW H_2-N_2 Arcjet Thruster," *Plasma science and Technology,* vol. 12, pp. 473-477, Aug 2010.

[4] W. Pan, *et al.*, "Arc root attachment on the anode surface of arc plasma torch observed with a novel method," *Chinese Physics Letters,* vol. 22, pp. 2895-2898, Nov 2005.